

# SCIENTIFIC REPORTS



OPEN

## Effect of Unsaturated Sn Atoms on Gas-Sensing Property in Hydrogenated SnO<sub>2</sub> Nanocrystals and Sensing Mechanism

Y. Yuan<sup>1</sup>, Y. Wang<sup>1</sup>, M. Wang<sup>1</sup>, J. Liu<sup>1</sup>, C. Pei<sup>1</sup>, B. Liu<sup>1</sup>, H. Zhao<sup>1</sup>, S. Liu<sup>2</sup> & H. Yang<sup>1</sup>

Sensing reaction mechanism is crucial for enhancing the sensing performance of semiconductor-based sensing materials. Here we show a new strategy to enhancing sensing performance of SnO<sub>2</sub> nanocrystals by increasing the density of unsaturated Sn atoms with dangling bonds at the SnO<sub>2</sub> surface through hydrogenation. A concept of the surface unsaturated Sn atoms serving as active sites for the sensing reaction is proposed, and the sensing mechanism is described in detail at atomic and molecule level for the first time. Sensing properties of other metal oxide sensors and catalytic activity of other catalysts may be improved by using the hydrogenation strategy. The concept of the surface unsaturated metal atoms serving as active sites may be very useful for understanding the sensing and catalytic reaction mechanisms and designing advanced sensing sensors, catalysts and photoelectronic devices.

As an important n-type metal-oxide semiconductor with a band gap of 3.6 eV at 300 K<sup>1</sup>, tin dioxide (SnO<sub>2</sub>) is well known for its numerous potential applications in field emission<sup>2–4</sup>, lithium ion batteries<sup>5–7</sup>, photocatalysis<sup>8,9</sup>, dye-sensitized solar cells<sup>10,11</sup>, perovskite solar cells<sup>12–15</sup>, supercapacitors<sup>16,17</sup>, light emitting devices<sup>18</sup> and so on. On the other hand, SnO<sub>2</sub> is considered to be one of the best known gas-sensing materials due to its remarkable receptivity variation in gaseous environment and excellent chemical stability<sup>19–22</sup>. Over the past decades, with the development of nanoscience and nanotechnology, SnO<sub>2</sub> nanomaterials with controlled morphologies, including nanoring<sup>20</sup>, nanowires<sup>23,24</sup>, nanobelts<sup>25</sup>, nanotubes<sup>26,27</sup>, nanosheets<sup>28</sup>, hollow spheres<sup>29,30</sup>, flower-like structure<sup>31,32</sup>, nanopolyhedrons<sup>33</sup>, hierarchical nanoarchitectures<sup>34,35</sup>, octahedra<sup>21,22</sup> and porous nanospheres<sup>36</sup> have been employed to fabricate gas sensors for detection of inflammable and toxic gases and volatile organic compounds (VOC) to improve gas-sensing properties. It was found that sensitivity of the sensors based SnO<sub>2</sub> nanostructured materials is increased by exposing high-energy facets<sup>21,22</sup> and increasing surface area<sup>26,31,36</sup>. Additionally, the sensitivity and selectivity of SnO<sub>2</sub>-based sensors can be significantly improved through doping with Cu, and Zn elements<sup>37,38</sup>, decorating with Ag<sub>2</sub>O<sup>39</sup>, PdO<sup>40</sup>, Ag<sup>41</sup> and Pd<sup>42</sup> nanoparticles, and forming SnO<sub>2</sub>-ZnO heteronanostructures<sup>43</sup>.

Metal-oxide gas sensors like SnO<sub>2</sub> operate on the basis of the change of the electrical resistance upon exposure to air or a test gas<sup>44</sup>. The variations of the resistances are brought about by the oxidation-reduction reaction of the adsorbed oxygen with the test gas taking place on the metal-oxide surface<sup>45,46</sup>. For this reason, the sensing behaviors of metal oxides should be very sensitive to the surface adsorption oxygen ability of the sensing materials. The adsorption oxygen ability may be enhanced by increasing density of the unsaturated metallic atoms with dangling bonds on the surface of metal-oxide sensors through hydrogenation. However, such a strategy for increasing sensing properties has never been reported up to now.

<sup>1</sup>Shaanxi Key Laboratory for Advanced Energy Devices; Shaanxi Engineering Laboratory for Advanced Energy Technology; Key Laboratory of Macromolecular Science of Shaanxi Province, School of Materials Science and Engineering, Shaanxi Normal University, Xi'an, 710119, China. <sup>2</sup>Key Laboratory of Applied Surface and Colloid Chemistry, National Ministry of Education; Shaanxi Key Laboratory for Advanced Energy Devices; Shaanxi Engineering Lab for Advanced Energy Technology, School of Materials Science and Engineering, Shaanxi Normal University, Xi'an, 710119, China. Correspondence and requests for materials should be addressed to H.Y. (email: [hqyang@snnu.edu.cn](mailto:hqyang@snnu.edu.cn))

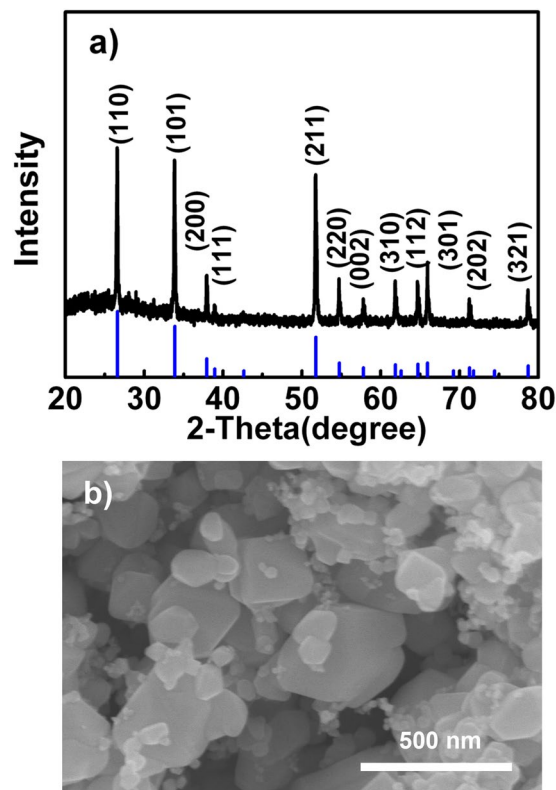


**Figure 1.** XRD and SEM characterizations of the SnO<sub>2</sub> samples without hydrogenation. (a) XRD pattern, (b) SEM image.

Herein, we demonstrated the enhanced volatile-organic-compound sensors based on the hydrogenated SnO<sub>2</sub> nanocrystals for the first time. The hydrogenated SnO<sub>2</sub> nanocrystals displayed far higher response towards ethanol, methanol and triethylamine than SnO<sub>2</sub> samples without hydrogenation, and the gas-sensing sensitivity was further increased with the hydrogenation time. The excellent gas-sensing performance arises from the increased density of the unsaturated Sn atoms with dangling bonds through hydrogenation, a concept of the unsaturated Sn atom serving as an active site for the sensing reaction is thus proposed, and a new sensing reaction mechanism is described in detail.

## Results

Morphology and crystal structure of SnO<sub>2</sub> samples. Figure 1a shows X-ray diffraction (XRD) pattern of the SnO<sub>2</sub> samples without hydrogenation. In the XRD pattern, all diffraction peaks were attributed to the pure tetragonal phase with cell constants of  $a = b = 4.738 \text{ \AA}$  and  $c = 3.187 \text{ \AA}$  (Joint Committee on Powder Diffraction Standards No. 41-1445). Scanning electron microscope (SEM) image shown in Fig. 1b indicated that the SnO<sub>2</sub> samples without hydrogenation consists of nanocrystals with irregular morphology and the sizes of 50–500 nm. The SnO<sub>2</sub> nanocrystals were hydrogenated for 5, 10 and 15 h at 150 °C, and the as-obtained sample was labeled SnO<sub>2</sub>-H-5, SnO<sub>2</sub>-H-10 and SnO<sub>2</sub>-H-15, respectively. The three kinds of hydrogenated samples were characterized with FESEM and XRD, and the results are shown in Supporting Information Fig. 1. It can be seen that after H<sub>2</sub> reduction the morphology and crystal structure of SnO<sub>2</sub> nanocrystals remain unchanged. The as-obtained hydrogenated samples still consist of rutile SnO<sub>2</sub> nanocrystals with various sizes.

Gas-sensing Performance. The transient response characteristics of the hydrogenated and non-hydrogenated SnO<sub>2</sub> nanocrystals to different concentrations of ethanol, methanol or triethylamine are displayed in Supporting Information Fig. 2. When the VOC was injected, the electric resistance of four types of SnO<sub>2</sub> nanocrystal sensors decreased suddenly, and then increased rapidly and recovered to their respective initial resistance after release of the VOC vapor. The resistance change of four kinds of SnO<sub>2</sub> nanocrystal sensors is in accordance with the typical sensing property of the n-type semiconductor<sup>32</sup>. Figure 2a–c shows sensing response curves of the three types of SnO<sub>2</sub> nanocrystal sensors to ethanol, methanol and triethylamine of different concentration, respectively. It can be clearly seen that the hydrogenated SnO<sub>2</sub> nanocrystal sensors have higher response than the nanocrystals without hydrogenation for three kinds of VOC vapors. The response value of SnO<sub>2</sub> sensors increases further with prolonging the hydrogenation time.

Moreover, to investigate stability of the sensor based on the SnO<sub>2</sub>-H-15, after the first measurement the hydrogenated SnO<sub>2</sub> sensor was stored in air and kept working at 350 °C for subsequent sensing property tests. After the sensor fabrication and aging for 7 days, a series of tests were conducted with 100 ppm of ethanol. The result was shown in Supporting Information Fig. 3. It was found that response value of the hydrogenated SnO<sub>2</sub> sensor

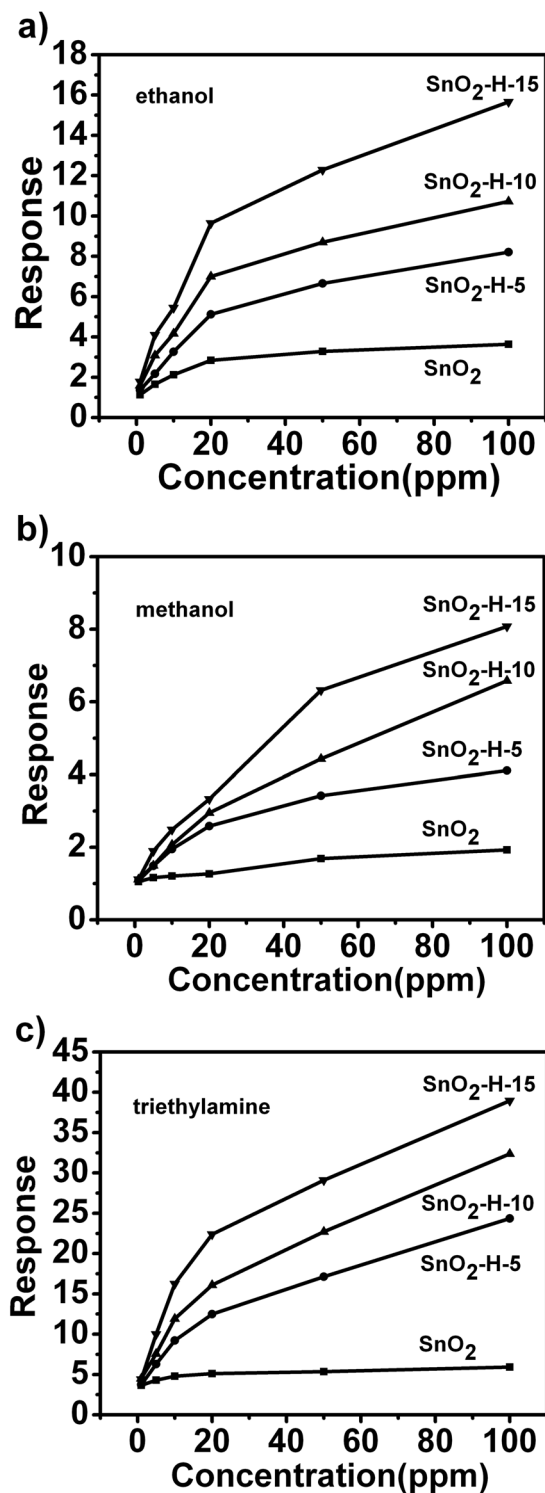


**Figure 2.** The response curves of the sensors based on the hydrogenated and non-hydrogenated SnO<sub>2</sub> nanocrystals to different concentrations of VOCs with 50% of relative humidity at 350 °C.

to 100 ppm of ethanol is between 18.9 and 20.5 during the test of 31 days, revealing that the hydrogenated SnO<sub>2</sub> sensor demonstrated good long-term stability.

### Discussion

It is well accepted that the resistance change of the metal oxide semiconductor based sensors like SnO<sub>2</sub> is based on the exchange of charges between the adsorbed gaseous species and the surface of metal oxide sensing materials<sup>20–22, 44, 47, 48</sup>. In order to understand the role of hydrogenation in the increase of response of SnO<sub>2</sub> nanocrystal sensor towards VOC, resistances of the four types of SnO<sub>2</sub> nanocrystal sensors in air and in ethanol vapors of

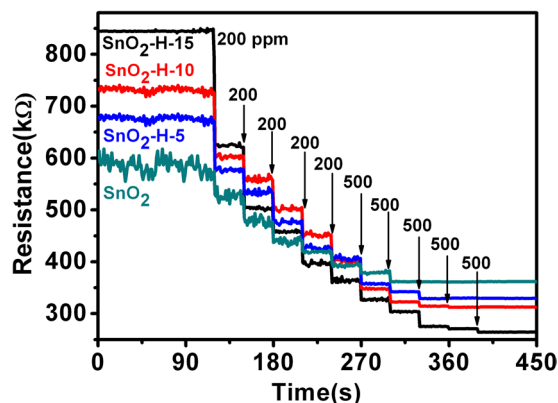


**Figure 3.** The resistance of the sensors based on the hydrogenated and non-hydrogenated SnO<sub>2</sub> nanocrystals in air and in different concentrations of ethanol vapors with of 50% relative humidity at 350 °C. The concentration labeled in the figure is the ethanol concentration of injection each time.

Samples	R <sub>a</sub> (kΩ)	R <sub>sg</sub> (kΩ)	The saturated concentration of ethanol (ppm)
SnO <sub>2</sub>	585.24	361.82	2000
SnO <sub>2</sub> -H-5	675.98	329.30	2500
SnO <sub>2</sub> -H-10	731.35	264.60	3000
SnO <sub>2</sub> -H-15	844.30	244.52	3500

**Table 1.** Resistances in air (R<sub>a</sub>) and in the saturated ethanol (R<sub>sg</sub>) and the ethanol saturated concentrations of the hydrogenated and non-hydrogenated SnO<sub>2</sub> samples.

different concentrations were measured, and the results are displayed in Fig. 3. It was found that the hydrogenated SnO<sub>2</sub> nanocrystal sensors have higher resistance values than SnO<sub>2</sub> samples without hydrogenation, and the resistance change follows the order of SnO<sub>2</sub>-H-15 > SnO<sub>2</sub>-H-10 > SnO<sub>2</sub>-H-5 > SnO<sub>2</sub>. The resistance values of the four types of SnO<sub>2</sub> sensors reduce with the injection of ethanol, and finally reach a constant value. The saturated ethanol concentrations for SnO<sub>2</sub>, SnO<sub>2</sub>-H-5, SnO<sub>2</sub>-H-10 and SnO<sub>2</sub>-H-15 are 2000, 2500, 3000 and 3500 ppm, respectively (Table 1). In the saturated ethanol vapor environment, the hydrogenated SnO<sub>2</sub> nanocrystal sensors have lower electric resistances than the sensors based on the SnO<sub>2</sub> samples without hydrogenation, and the resistance follows the order of SnO<sub>2</sub> > SnO<sub>2</sub>-H-5 > SnO<sub>2</sub>-H-10 > SnO<sub>2</sub>-H-15.

To determine the state of oxygen species on the surface of the hydrogenated and non-hydrogenated SnO<sub>2</sub> samples, X-ray photoelectron spectroscopy (XPS) analysis was carried out. Figure 4a–b shows the survey spectra, Sn 2p<sub>5/2</sub> and 2p<sub>3/2</sub> spectra, respectively. The binding energy of Sn 2p<sub>5/2</sub> and 2p<sub>3/2</sub> is identified at 486.12 and 494.52 eV, respectively (Fig. 4b). Figure 4c–f shows the O 1s spectra from the four kinds of SnO<sub>2</sub> samples. It was clearly observed that all O 1s XPS peaks can be decomposed into three Gaussian components centered at about 529, 531, and 533 eV, respectively. The three components are indexed to O<sup>2-</sup> ions in SnO<sub>2</sub> lattice (O<sub>L</sub>), O<sup>2-</sup> ions in oxygen-deficient regions (O<sub>V</sub>) and chemisorbed oxygen (O<sub>C</sub>) species and –OH groups, respectively<sup>46,49</sup>. Intensities of O<sub>V</sub> and O<sub>C</sub> from the SnO<sub>2</sub>-H-5, SnO<sub>2</sub>-H-10 and SnO<sub>2</sub>-H-15 are higher than those from SnO<sub>2</sub> samples without hydrogenation. The relative percentages of the O<sub>L</sub> and O<sub>V</sub> components as well as O<sub>C</sub> and –OH mixed components from the SnO<sub>2</sub>-H-5, SnO<sub>2</sub>-H-10, SnO<sub>2</sub>-H-15 and SnO<sub>2</sub> are summarized in Supplementary Table 1. It is apparent that the relative percentages of the O<sub>V</sub> components as well as O<sub>C</sub> and –OH mixed components of the SnO<sub>2</sub> nanocrystals can be increased through hydrogenation. Additionally, IR spectra of the four kinds of SnO<sub>2</sub> nanocrystal samples were investigated and the results are shown in Fig. 5. The band at about 3500 cm<sup>-1</sup> is attributed to the asymmetrical stretching vibration of O–H group. Apparently, the hydrogenated SnO<sub>2</sub> nanocrystals had lower intensities of the O–H vibration model than SnO<sub>2</sub> samples without hydrogenation, and the O–H vibration intensity reduced further with increasing hydrogenation time. Therefore, the hydrogenated SnO<sub>2</sub> samples have higher relative percentage of O<sub>C</sub> components compared with SnO<sub>2</sub> samples without hydrogenation, and the relative percentage of O<sub>C</sub> components further increases with the hydrogenation time. On basis of the experimental results, we concluded that the enhanced sensing property of the hydrogenated SnO<sub>2</sub> VOC sensors may derive from the increase on the relative percentages of the O<sub>V</sub> and O<sub>C</sub> components and the decrease in the amount of O–H groups.

When SnO<sub>2</sub> nanocrystals were hydrogenated, the O–H groups and O ions at the surface reacted with H<sub>2</sub> to form H<sub>2</sub>O, and thus more the unsaturated Sn atoms with dangling bonds were formed at the SnO<sub>2</sub> surface, as a result, density of unsaturated Sn atoms with dangling bonds increases at the surface, as shown in Fig. 6a. Therefore, we considered that the unsaturated Sn atoms with dangling bonds at the surface may play a pivotal role in the enhancement of gas-sensing property. The surface unsaturated Sn atoms with dangling bonds may serve as an active site for the sensing reaction.

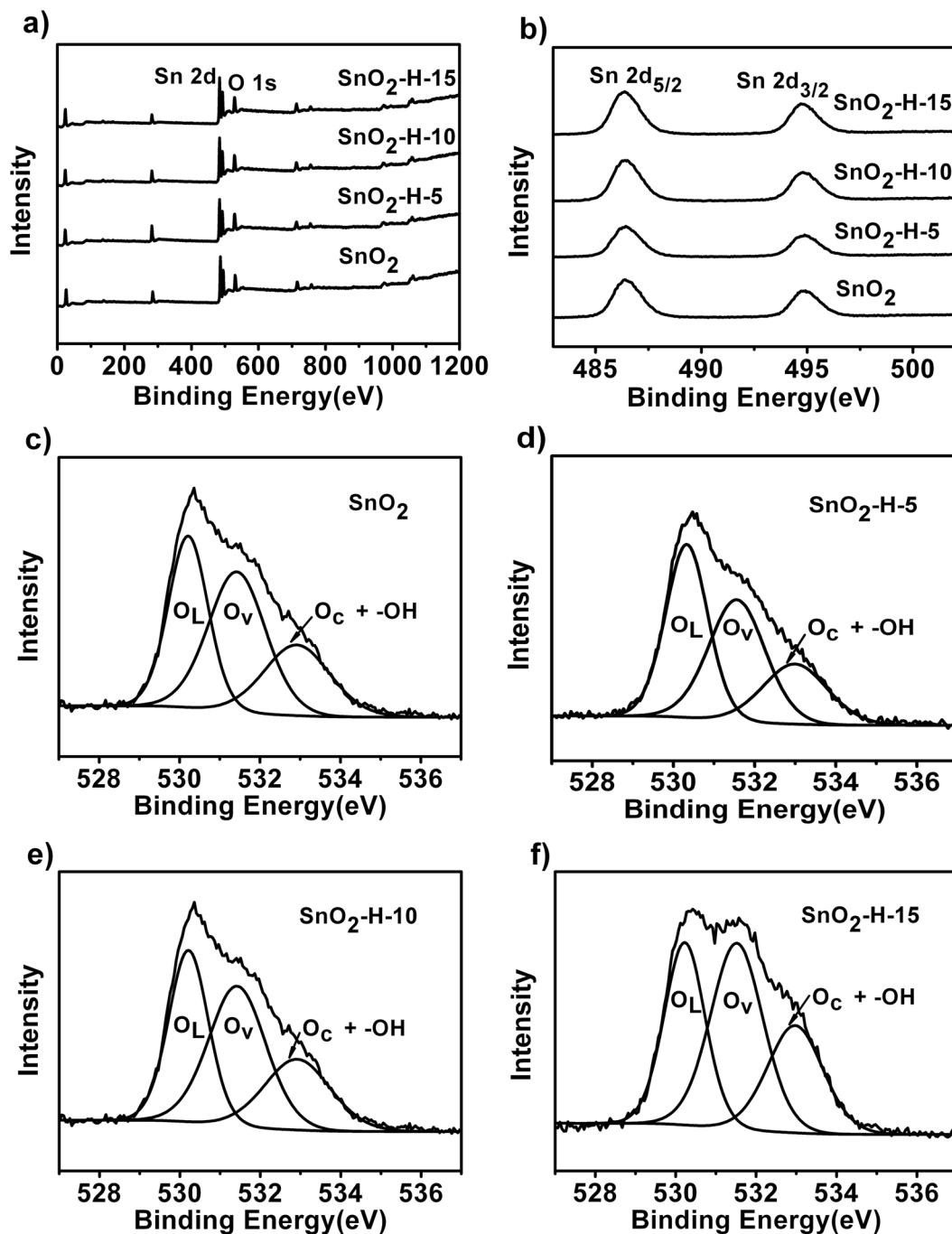


**Figure 4.** XPS Characterizations of the hydrogenated and non-hydrogenated SnO<sub>2</sub> nanocrystals. (a) The survey spectra. (b) Sn 2d<sub>5/2</sub>, 2d<sub>3/2</sub> and (c–f) O 1s spectra of (c) SnO<sub>2</sub>, (d) SnO<sub>2</sub>-H-5, (e) SnO<sub>2</sub>-H-10 and (f) SnO<sub>2</sub>-H-15.

As we know, SnO<sub>2</sub> is a typical n-type semiconductor sensing material with oxygen vacancies, in which electrons participate in the electric conduction process<sup>50,51</sup>. Like ZnO<sup>52</sup>, TiO<sub>2</sub><sup>53</sup> and Fe<sub>2</sub>O<sub>3</sub><sup>54</sup>, the loss of oxygen in SnO<sub>2</sub> create non-contributing (extra) electrons. As shown in Fig. 6a, the presence of oxygen vacancies necessarily led to the production of the unsaturated Sn atoms with dangling bonds, and thus we consider that the Sn atoms with dangling bonds can provide free electrons. In air, the unsaturated Sn atoms with dangling bonds at the surface of SnO<sub>2</sub> sensing material have reducing capacity and adsorb oxygen molecules due to the deficiency of oxygen. The adsorbed oxygen molecules have good oxidation capacity and can draw free electrons in SnO<sub>2</sub> sensing material, the electrons captured by the adsorbed oxygen can not participate in the electric conduction process. As a result, the number of free electrons within SnO<sub>2</sub> decreases, and the SnO<sub>2</sub> sensing material thus shows a high resistance state, as shown in Fig. 6b. The density of unsaturated Sn atoms with dangling bonds increase at the SnO<sub>2</sub> surface is increased through hydrogenation (Fig. 6a), and thus the amounts of the adsorbed oxygen and the electrons

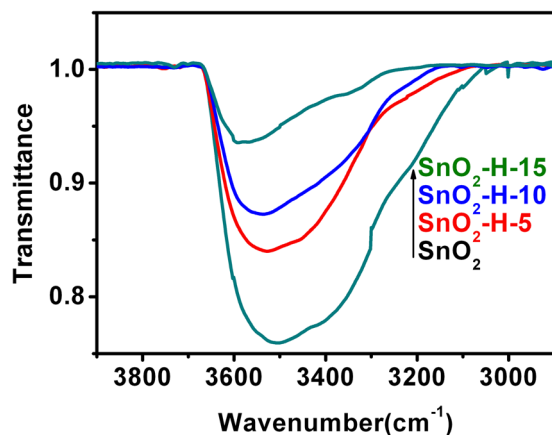


**Figure 5.** IR spectra of the hydrogenated and non-hydrogenated SnO<sub>2</sub> nanocrystals.

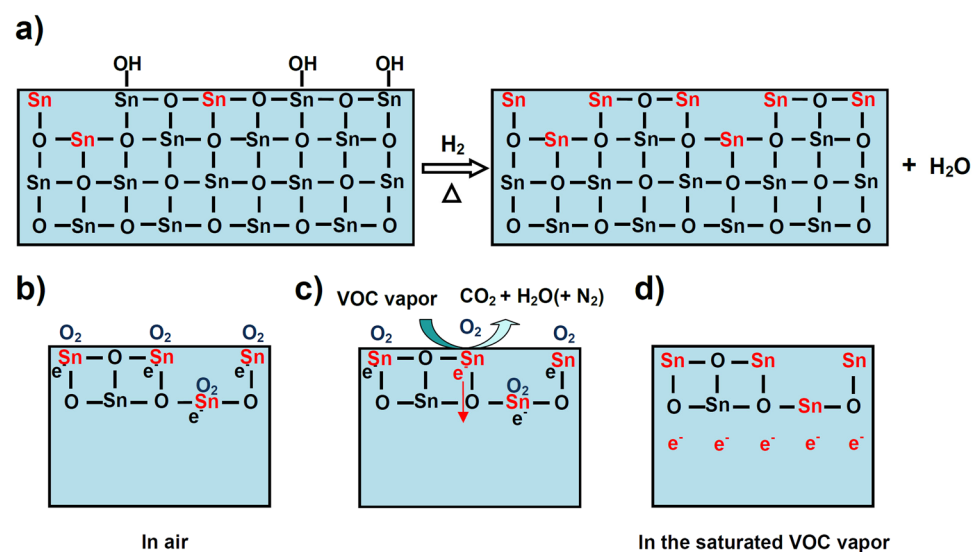


**Figure 6.** Schematic diagrams of sensing mechanism. (a) Hydrogenation reaction of SnO<sub>2</sub> nanocrystals. (b–d) Sensing reaction mechanism of the hydrogenated SnO<sub>2</sub> nanocrystals at atomic and molecule level. The black e<sup>−</sup> and red e<sup>−</sup> represent the absorbed electrons by O<sub>2</sub> and free electrons, respectively.

captured by the adsorbed oxygen are enhanced. Therefore, in comparison with SnO<sub>2</sub> samples without hydrogenation, the hydrogenated SnO<sub>2</sub> samples have less free electrons and show higher resistance. When the SnO<sub>2</sub> sensor is exposed to a VOC vapor, the VOC gas molecules are oxidized into CO<sub>2</sub> and H<sub>2</sub>O (H<sub>2</sub>O + N<sub>2</sub>) by surface-adsorbed oxygen molecules, and thus the adsorbed oxygen was removed<sup>47,48</sup>. The electrons captured by the adsorbed oxygen molecules are released into SnO<sub>2</sub>, the number of free electrons in SnO<sub>2</sub> increases, and thus resistance value reduces, as shown in Fig. 6c. In the saturated VOC vapor, all the adsorbed oxygen molecules are removed, all the electrons captured by the adsorbed oxygen became into free electrons, and thus the electric resistance value is constant and the smallest, as shown in Fig. 6d. A total of electron in SnO<sub>2</sub> sensing materials can be increased with an increase on the density of unsaturated Sn atoms with dangling bonds at the SnO<sub>2</sub> surface because that the Sn atoms with dangling bonds can provide extra electrons. Therefore, in the saturated ethanol, the hydrogenated SnO<sub>2</sub> nanocrystals with higher densities of unsaturated Sn atoms with dangling bonds have more free electrons and lower electric resistances than SnO<sub>2</sub> samples without hydrogenation. Moreover, based on the experimental results in Fig. 3, we considered that the unsaturated Sn atoms with dangling bonds at SnO<sub>2</sub> surface can catalyze the reaction of the chemisorbed oxygen with the VOC molecules. The hydrogenated SnO<sub>2</sub> nanocrystal sensors have higher density of sensing reaction active sites (the unsaturated Sn atoms with dangling bonds) than SnO<sub>2</sub> samples without hydrogenation, and thus demonstrate higher response towards the VOC vapors.

In summary, the hydrogenated SnO<sub>2</sub> nanocrystals exhibit superior gas-sensing performance, compared with SnO<sub>2</sub> samples without hydrogenation. The enhanced sensing performances originate from the increased density of the unsaturated Sn atoms with dangling bonds at the SnO<sub>2</sub> surface through hydrogenation. The unsaturated Sn atoms with dangling bonds are regarded as active sites of the sensing reaction, and the sensing mechanism is



firstly elaborated at atomic and molecule level. The hydrogenation may be a general strategy for improving sensing performances of metal oxide sensors and catalytic activities of catalysts. The concept of the unsaturated metal atoms with dangling bonds serving as the reaction active sites not only can deepen understanding of the sensing and catalytic reaction mechanisms, but also provides new insights into the design and fabrication of highly efficient sensing materials, catalysts and photoelectronic devices.

## Methods

**Preparation of samples.** SnO<sub>2</sub> nanocrystals were purchased from Sinopharm Chemical Reagent Co., Ltd. (Shanghai, China). SnO<sub>2</sub> nanocrystals were hydrogenated: 100 mg of SnO<sub>2</sub> nanocrystals were heated in a horizontal furnace and maintained at 150 °C for 5, 10 or 15 h under a H<sub>2</sub> gas flow to obtain hydrogenated SnO<sub>2</sub> nanocrystals.

**Characterization of SnO<sub>2</sub> samples.** The crystal structure of the hydrogenated and non-hydrogenated SnO<sub>2</sub> nanocrystals were characterized by X-ray diffraction (Haoyuan DX-2700, Dandong, China) using Cu K $\alpha$ 1 radiation with 2 $\theta$  ranging from 20° to 80°. The morphology was analyzed by field-emission scanning electron microscope (Hitachi SU8020, Japan) with an acceleration voltage of 20 kV. The surface compositions were determined on an X-ray photoelectron spectroscopy (Kratos Axis ultra, Japan) and on an infrared (IR) spectrometer (Bruker Tensor 27, Germany) by mixing 0.001 g of sample with 0.100 g of KBr and pressing into tablet.

**Gas-sensing measurements.** Measurements on gas sensitivity of SnO<sub>2</sub> samples were performed using a WS-30A system (Weisheng Instruments Co., Zhengzhou, China). In a typical test, a sensor was fabricated by coating a certain amount of SnO<sub>2</sub> paste (consisting of SnO<sub>2</sub> nanocrystals and the terpeneol solvent) onto a ceramic tube with Au electrodes and Pt conducting wires. A Ni-Cr filament was inserted in the tube as a heater element to provide the operation temperature from 200 to 400 °C. To improve the device's stability, the as-prepared SnO<sub>2</sub> sensors were aged at 350 °C for 7 days before testing. Measurement of gas-sensing property has been described in the reference<sup>32</sup>. The response of the SnO<sub>2</sub> sensor is defined as the ratio  $R_a/R_g$ , where  $R_a$  and  $R_g$  are the resistances of the sensor in air and in the test gas at the operation temperature of about 350 °C, respectively.

**Data availability.** The data that support the findings of this study are available from the corresponding author upon request.

## References

- Zhu, L. L., Hong, M. H. & Ho, G. W. Hierarchical assembly of SnO<sub>2</sub>/ZnO nanostructures for enhanced photocatalytic performance. *Sci. Rep.* **5**, 11609 (2015).
- He, H. *et al.* Beaklike SnO<sub>2</sub> nanorods with strong photoluminescent and field-emission properties. *Small* **2**, 116–120 (2006).
- Ding, J. J. *et al.* Enhancement of field emission and photoluminescence properties of graphene-SnO<sub>2</sub> composite nanostructures. *ACS Appl. Mater. Interfaces* **3**, 4299–4305 (2011).
- Wang, X. *et al.* Low-temperature vapor–solid growth and excellent field emission performance of highly oriented SnO<sub>2</sub> nanorod arrays. *Acta Mater.* **59**, 1291–1299 (2011).
- Wang, Y. *et al.* Designed hybrid nanostructure with catalytic effect: beyond the theoretical capacity of SnO<sub>2</sub> anode material for lithium ion batteries. *Sci. Rep.* **5**, 9164 (2015).
- Park, M. S. *et al.* Preparation and electrochemical properties of SnO<sub>2</sub> nanowires for application in lithium-ion batteries. *Angew. Chem. Int. Ed.* **46**, 750–753 (2007).
- Wu, H. B., Chen, J. S., Lou, X. W. & Hng, H. H. Synthesis of SnO<sub>2</sub> hierarchical structures assembled from nanosheets and their lithium storage properties. *J. Phys. Chem. C* **115**, 24605–24610 (2011).
- Huang, X. *et al.* Type-II ZnO nanorod-SnO<sub>2</sub> nanoparticle heterostructures: characterization of structural, optical and photocatalytic properties. *Nanoscale* **5**, 3828–3833 (2013).
- Li, P. *et al.* Iodinated SnO<sub>2</sub> quantum dots: A facile and efficient approach to increase solar absorption for visible-light photocatalysis. *J. Phys. Chem. C* **120**, 9253–9262 (2016).
- Dong, Z. H. *et al.* Quintuple-shelled SnO<sub>2</sub> hollow microspheres with superior light scattering for high-performance dye-sensitized solar cells. *Adv. Mater.* **26**, 905–909 (2014).
- Ahn, S. H., Kim, D. J., Chi, W. S. & Kim, J. H. One-dimensional hierarchical nanostructures of TiO<sub>2</sub> nanosheets on SnO<sub>2</sub> nanotubes for high efficiency solid-state dye-sensitized solar cells. *Adv. Mater.* **25**, 4893–4897 (2013).
- Song, J. X. *et al.* Low-temperature SnO<sub>2</sub>-based electron selective contact for efficient and stable perovskite solar cells. *J. Mater. Chem. A* **3**, 10837–10844 (2015).
- Ke, W. J. *et al.* Low-temperature solution-processed tin oxide as an alternative electron transporting layer for efficient perovskite solar cells. *J. Am. Chem. Soc.* **137**, 6730–6733 (2015).
- Zhu, Z. L. *et al.* Mesoporous SnO<sub>2</sub> single crystals as an effective electron collector for perovskite solar cells. *Phys. Chem. Chem. Phys.* **17**, 18265–18268 (2015).
- Dong, Q. S. *et al.* Insight into perovskite solar cells based on SnO<sub>2</sub> compact electron-selective layer. *J. Phys. Chem. C* **119**, 10212–10217 (2015).
- Zhang, Y. D. *et al.* Growth of 3D SnO<sub>2</sub> nanosheets on carbon cloth as a binder-free electrode for supercapacitors. *J. Mater. Chem. A* **3**, 15057–15067 (2015).
- Li, Z. J., Chang, T. Q., Yun, G. Q., Guo, J. & Yang, B. C. 2D tin dioxide nanoplatelets decorated graphene with enhanced performance supercapacitor. *J. Alloys Compd.* **586**, 353–359 (2014).
- Brovelli, S. *et al.* Fully inorganic oxide-in-oxide ultraviolet nanocrystal light emitting devices. *Nat. Commun.* **3**, 690 (2012).
- Kuang, Q., Lao, C. S., Wang, Z. L., Xie, Z. X. & Zheng, L. S. High-sensitivity humidity sensor based on a single SnO<sub>2</sub> nanowire. *J. Am. Chem. Soc.* **129**, 6070–6071 (2007).
- Li, S. H. *et al.* Highly sensitive gas sensor based on SnO<sub>2</sub> nanorings for detection of isopropanol. *J. Alloys Compd.* **688**, 712–717 (2016).
- Han, X. G. *et al.* Synthesis of tin dioxide octahedral nanoparticles with exposed high-energy {221} facets and enhanced gas-sensing properties. *Angew. Chem. Int. Ed.* **48**, 9180–9183 (2009).
- Wang, X. *et al.* Controlled synthesis and enhanced catalytic and gas-sensing properties of tin dioxide nanoparticles with exposed high-energy facets. *Chem. Eur. J* **18**, 2283–2289 (2012).
- Kolmakov, A., Zhang, Y. X., Cheng, G. S. & Moskovits, M. Detection of CO and O<sub>2</sub> using tin oxide nanowire sensors. *Adv. Mater.* **12**, 997–1000 (2003).

24. Wang, Y. L., Jiang, X. C. & Xia, Y. N. A solution-phase, precursor route to polycrystalline SnO<sub>2</sub> nanowires that can be used for gas sensing under ambient conditions. *J. Am. Chem. Soc.* **125**, 16176–16177 (2003).
25. Fields, L. L., Zheng, J. P., Cheng, Y. & Xiong, P. Room-temperature low-power hydrogen sensor based on a single tin dioxide nanobel. *Appl. Phys. Lett.* **88**, 263102 (2006).
26. Zhang, J., Guo, J., Xu, H. Y. & Cao, B. Q. Reactive-template fabrication of porous SnO<sub>2</sub> nanotubes and their remarkable gas-sensing performance. *ACS Appl. Mater. Interfaces* **5**, 7893–7898 (2013).
27. Shi, L. & Lin, H. L. Preparation of band gap tunable SnO<sub>2</sub> nanotubes and their ethanol sensing properties. *Langmuir* **27**, 3977–3981 (2011).
28. Sun, P. *et al.* Porous SnO<sub>2</sub> hierarchical nanosheets: hydrothermal preparation, growth mechanism, and gas sensing properties. *CrystEngComm* **13**, 3718–3724 (2011).
29. Gyger, F., Hübner, M., Feldmann, C., Barsan, N. & Weimar, U. Nanoscale SnO<sub>2</sub> hollow spheres and their application as a gas-sensing material. *Chem. Mater.* **22**, 4821–4827 (2010).
30. Zhang, J. *et al.* Polypyrrole-coated SnO<sub>2</sub> hollow spheres and their application for ammonia sensor. *J. Phys. Chem. C* **113**, 1662–1665 (2009).
31. Wang, H. *et al.* Preparation of flower-like SnO<sub>2</sub> nanostructures and their applications in gas-sensing and lithium storage. *Cryst. Growth Des.* **11**, 2942–2947 (2011).
32. Liu, B., Zhang, L. H., Zhao, H., Chen, Y. & Yang, H. Q. Synthesis and sensing properties of spherical flowerlike architectures assembled with SnO<sub>2</sub> submicron rods. *Sens. Actuators, B* **173**, 643–651 (2012).
33. Chen, D., Xu, J., Xie, Z. & Shen, G. Z. Nanowires assembled SnO<sub>2</sub> nanopolyhedrons with enhanced gas sensing properties. *ACS Appl. Mater. Interfaces* **3**, 2112–2117 (2011).
34. Liu, Y. *et al.* Hierarchical SnO<sub>2</sub> nanostructures made of intermingled ultrathin nanosheets for environmental remediation, smart gas sensor, and supercapacitor applications. *ACS Appl. Mater. Interfaces* **6**, 2174–2184 (2014).
35. Jiang, L. Y., Wu, X. L., Guo, Y. G. & Wan, L. J. SnO<sub>2</sub>-based hierarchical nanomicrostructures: facile synthesis and their applications in gas sensors and lithium-ion batteries. *J. Phys. Chem. C* **113**, 14213–14219 (2009).
36. Manjula, P., Boppella, R. & Manorama, S. V. A facile and green approach for the controlled synthesis of porous SnO<sub>2</sub> nanospheres: application as an efficient photocatalyst and an excellent gas sensing material. *ACS Appl. Mater. Interfaces* **4**, 6252–6260 (2012).
37. Jin, W. X. *et al.* One-step synthesis and highly gas-sensing properties of hierarchical Cu-doped SnO<sub>2</sub> nanoflowers. *Sens. Actuators, B* **213**, 171–180 (2015).
38. Zhao, Q. Q. *et al.* Morphology-modulation of SnO<sub>2</sub> hierarchical architectures by Zn doping for glycol gas sensing and photocatalytic applications. *Sci. Rep.* **5**, 7874 (2015).
39. Chen, X. *et al.* Templating synthesis of SnO<sub>2</sub> nanotubes loaded with Ag<sub>2</sub>O nanoparticles and their enhanced gas sensing properties. *Adv. Funct. Mater.* **21**, 2049–2056 (2011).
40. Zhu, Y. F. *et al.* A facile synthesis of PdO-decorated SnO<sub>2</sub> nanocomposites with open porous hierarchical architectures for gas sensors. *J. Am. Ceram. Soc.* **99**, 3770–3774 (2016).
41. Hwang, I. S. *et al.* Facile control of C<sub>2</sub>H<sub>5</sub>OH sensing characteristics by decorating discrete Ag nanoclusters on SnO<sub>2</sub> nanowire networks. *ACS Appl. Mater. Interfaces* **3**, 3140–3145 (2011).
42. Yang, D. J., Kamienschick, I., Youn, Y. D., Rothschild, A. & Kim, I. D. Ultrasensitive and highly selective gas sensors based on electrospun SnO<sub>2</sub> nanofibers modified by Pd loading. *Adv. Funct. Mater.* **20**, 4258–4264 (2010).
43. Fu, D. Y., Zhu, C. L., Zhang, X. T., Li, C. Y. & Chen, Y. J. Two-dimensional net-like SnO<sub>2</sub>/ZnO heterostructures for high-performance H<sub>2</sub>S gas sensor. *J. Mater. Chem. A* **4**, 1390–1398 (2016).
44. Morrison, S. R. Semiconductor gas sensors. *Sens. Actuators* **2**, 329–341 (1982).
45. Gardon, M. & Guilemany, J. M. A review on fabrication, sensing mechanisms and performance of metal oxide gas sensors. *J. Mater. Sci: Mater. Electron* **24**, 1410–1421 (2013).
46. Han, X. G. *et al.* Controlling morphologies and tuning the related properties of nano/microstructured ZnO crystallites. *J. Phys. Chem. C* **113**, 584–589 (2009).
47. Liu, B. *et al.* Synthesis and enhanced gas-sensing properties of ultralong NiO nanowires assembled with NiO nanocrystals. *Sens. Actuators, B* **156**, 251–262 (2011).
48. Li, L. *et al.* Hydrothermal synthesis and gas sensing properties of single-crystalline ultralong ZnO nanowires. *Appl. Phys. A* **98**, 635–641 (2010).
49. Li, C. C., Yin, X. M., Li, Q. H. & Wang, T. H. Enhanced gas sensing properties of ZnO/SnO<sub>2</sub> hierarchical architectures by glucose-induced attachment. *CrystEngComm* **13**, 1557–1563 (2011).
50. Wang, Y., Zhang, H. & Sun, X. H. Electrospun nanowebbs of NiO/SnO<sub>2</sub> p-n heterojunctions for enhanced gas sensing. *Appl. Surf. Sci.* **389**, 514–520 (2016).
51. Law, M., Kind, H., Messer, B., Kim, F. & Yang, P. D. Photochemical sensing of NO<sub>2</sub> with SnO<sub>2</sub> nanoribbon nanosensors at room temperature. *Angew. Chem. Int. Ed.* **41**, 2405–2408 (2002).
52. Kim, H. S. *et al.* Effects of oxygen concentration on the electrical properties of ZnO films. *Ceram. Int.* **34**, 1097–1101 (2008).
53. Pan, X. Y., Yang, M. Q., Fu, X. Z., Zhang, N. & Xu, Y. J. Defective TiO<sub>2</sub> with oxygen vacancies: synthesis, properties and photocatalytic applications. *Nanoscale* **5**, 3601–3614 (2013).
54. Gurlo, A., Sahn, M., Opera, A., Barsan, N. & Weimar, U. A p- to n-transition on α-Fe<sub>2</sub>O<sub>3</sub>-based thick film sensors studied by conductance and work function change measurements. *Sens. Actuators, B* **102**, 291–298 (2004).

## Acknowledgements

This work was supported by the National Natural Science Foundation of China (Grant Nos 21073116 and 21501116), and the Fundamental Research Funds for the Central Universities (GK 201601003).

## Author Contributions

Y.K.Y. and H.Q.Y. are responsible for all phases of the research. Y.K.Y. prepared the samples and performed the characterizations of XRD, FESEM and XPS and the gas-sensing property measurement. Y.W., M.W., and J.F.L. assisted with the IR characterization. C.J.P., B.L., H.Z. and S.Z.L. helped with the data analysis. Y.K.Y. wrote the initial draft, H.Q.Y. revised the final draft.

## Additional Information

**Supplementary information** accompanies this paper at doi:10.1038/s41598-017-00891-5

**Competing Interests:** The authors declare that they have no competing interests.

**Publisher's note:** Springer Nature remains neutral with regard to jurisdictional claims in published maps and institutional affiliations.





**Open Access** This article is licensed under a Creative Commons Attribution 4.0 International License, which permits use, sharing, adaptation, distribution and reproduction in any medium or format, as long as you give appropriate credit to the original author(s) and the source, provide a link to the Creative Commons license, and indicate if changes were made. The images or other third party material in this article are included in the article's Creative Commons license, unless indicated otherwise in a credit line to the material. If material is not included in the article's Creative Commons license and your intended use is not permitted by statutory regulation or exceeds the permitted use, you will need to obtain permission directly from the copyright holder. To view a copy of this license, visit <http://creativecommons.org/licenses/by/4.0/>.

© The Author(s) 2017